

New searches for H I 21 cm in damped Lyman α absorption systems

S. J. Curran,^{1*} P. Tzanavaris,^{2,3,4} J. K. Darling,⁵ M. T. Whiting,⁶ J. K. Webb,¹
C. Bignell,⁷ R. Athreya⁸ and M. T. Murphy⁹

¹*School of Physics, University of New South Wales, Sydney, NSW 2052, Australia*

²*Institute of Astronomy and Astrophysics, National Observatory of Athens, I. Metaxa and V. Paulou 152 36 Penteli, Greece*

³*Department of Physics and Astronomy, Johns Hopkins University, Baltimore, MD 21218, USA*

⁴*Laboratory for X-Ray Astrophysics, NASA Goddard Space Flight Center, Code 662, Greenbelt, MD 20771, USA*

⁵*Department of Astrophysical and Planetary Sciences, University of Colorado at Boulder, Boulder, Colorado 80309, USA*

⁶*CSIRO Australia Telescope National Facility, PO Box 76, Epping NSW 1710, Australia*

⁷*National Radio Astronomy Observatory, PO Box 2, Rt. 28/92 Green Bank, WV 24944-0002, USA*

⁸*National Centre for Radio Astrophysics, Pune 411 007, Maharashtra, India*

⁹*Centre for Astrophysics and Supercomputing, Swinburne University of Technology, PO Box 218, Hawthorn, VIC 3122 Australia*

Accepted 2009 October 15. Received 2009 October 15; in original form 2009 July 28

ABSTRACT

We present the results of three separate searches for H I 21-cm absorption in a total of 12 damped Lyman α absorption systems (DLAs) and sub-DLAs over the redshift range $z_{\text{abs}} = 0.86\text{--}3.37$. We find no absorption in the five systems for which we obtain reasonable sensitivities and add the results to those of other recent surveys in order to investigate factors which could have an effect on the detection rate. We provide evidence that the mix of spin temperature/covering factor ratios seen at low redshift may also exist at high redshift, with a correlation between the 21-cm line strength and the total neutral hydrogen column density, indicating a roughly constant spin temperature/covering factor ratio for all of the DLAs searched. Also, by considering the geometry of a flat expanding Universe together with the projected sizes of the background radio emission regions, we find, for the detections, that the 21-cm line strength is correlated with the size of the absorber. For the non-detections, it is apparent that larger absorbers (covering factors) are required in order to exhibit 21-cm absorption, particularly if these DLAs do not arise in spiral galaxies. We also suggest that the recent $z_{\text{abs}} = 2.3$ detection towards TXS 0311+430 arises in a spiral galaxy, but on the basis of a large absorption cross-section and high metallicity, rather than a low spin temperature.

Key words: galaxies: high redshift – galaxies: ISM – quasars: absorption lines – cosmology: observations – radio lines: galaxies.

1 INTRODUCTION

Damped Lyman α absorption systems (DLAs) are believed to be the precursors of modern-day galaxies, containing at least 80 per cent of the neutral gas mass density of the Universe (Prochaska, Herbert-Fort & Wolfe 2005). As the name suggests, DLAs are identified through their heavily damped absorption features, due to the large columns of neutral hydrogen ($N_{\text{HI}} \geq 2 \times 10^{20} \text{ cm}^{-2}$) through which the background quasar is viewed. The 21-cm spin-flip transition is of interest since it traces the cool component of the gas, with the comparison of the 21-cm absorption strength to the total neutral hydrogen column giving the gas spin temperature (T_{spin}) for a fully absorbed emission region ($f = 1$) (see equation 1, Section 3.1). Searches for 21-cm absorption in DLAs exhibit an

≈ 50 per cent detection rate, the detections occurring predominately at low redshift ($z_{\text{abs}} \lesssim 1$), suggesting an increase in the T_{spin}/f ratio with redshift, which could be due to higher spin temperatures and/or lower covering factors.

In order to shed light on which is the predominant factor, we have undertaken searches with the Green Bank Telescope (GBT) and Giant Metrewave Radio Telescopes (GMRT). In particular, we aim to:

- (i) Test the hypothesis of Curran et al. (2005) that 21-cm absorption should be readily detectable at high redshift, despite the large T_{spin}/f ratios, by searching for 21-cm absorption in DLAs which lie towards compact radio sources.
- (ii) Test the hypothesis of Curran et al. (2007b) that the spin temperature does not continue to increase with redshift, by searching in previously unsearched high-redshift ($z_{\text{abs}} \gtrsim 3.2$) DLAs.

*E-mail: sjc@phys.unsw.edu.au

(iii) Test the line strength–metallicity correlation (T_{spin}/f –[M/H] anticorrelation) of Curran et al. (2007b), which suggests that several, currently undetected, DLAs should be readily detectable in 21-cm absorption.

We have observed a dozen DLAs and sub-DLAs, and in this paper we present and discuss the results in the context of the above issues.

2 SAMPLE SELECTION AND OBSERVATIONS

2.1 GBT 2006 observations

2.1.1 Motivation

Prior to the recent high-redshift detections (Kanekar et al. 2006, 2007; York et al. 2007, discussed below), all of the DLAs detected in 21-cm absorption were at redshifts of $z_{\text{abs}} \lesssim 2$, where there is also an approximately equal number of non-detections. Kanekar & Chengalur (2003) interpreted this as the low-redshift DLAs having a mix of spin temperatures, whereas the high-redshift absorbers have exclusively high spin temperatures. However, all of the $z_{\text{abs}} \gtrsim 1$ absorbers have large DLA to quasi-stellar object (QSO) angular diameter distance ratios ($DA_{\text{DLA}}/DA_{\text{QSO}} \approx 1$), whereas the $z_{\text{abs}} \lesssim 1$ absorbers have a mix of ratios, due to the geometry effects of a flat expanding Universe (Curran & Webb 2006): those with low ratios are almost always detected in 21-cm absorption, whereas those with high ratios tend not to be detected, which is how the ‘spin temperature’ distribution of Kanekar & Chengalur (2003) is segregated. This strongly suggests, on the grounds of geometry alone and not allowing for various absorber and emitter sizes, that the covering factor, rather than the spin temperature, is the crucial criterion in determining the detectability of 21-cm absorption, where an absorber at high redshift will always cover the background quasar much less effectively than an equivalent absorber–quasar system at low redshift. Furthermore, Curran et al. (2005) had previously suggested that the non-detections at high redshift could be due to low covering factors, as opposed to elevated spin temperatures, and so 21-cm absorption should be readily detectable in high-redshift DLAs towards very compact radio sources.

With the GBT, we therefore embarked upon a survey for H I 21-cm absorption in the known radio-illuminated DLAs yet to be searched, prioritized by a small radio source size. For this, we used the Sloan Digital Sky Survey Damped Ly α Survey Data Release 1 (Prochaska & Herbert-Fort 2004) combined with the previously unsearched systems (Curran et al. 2002), giving 57 DLAs occulting radio-loud ($S \gtrsim 0.1$ Jy) quasars. We then shortlisted the DLAs and sub-DLAs in which the 21-cm transition was redshifted into the Prime Focus 342 and 450 MHz bands and which were located towards the four most compact radio sources – B3 0758+475 (SDSS J080137.67+472528.2), PKS 1402+044, PKS B1418–064 and PKS 2136+141 (Table 1, where we also give the radio source sizes for the other objects searched).

2.1.2 Observations and data reduction

The observations were performed with the GBT PF1 342 and 450 MHz receivers in position switching mode (level-3 sampling, one spectral window and dual polarization). The backend was either the GBT spectrometer using 32 768 lags over a 12.5 MHz band, giving a channel spacing of 381.47 Hz, or when radio frequency interference (RFI) appeared to be particularly bad, the spectral pro-

Table 1. The radio source sizes at ν_{θ} of the QSOs illuminating the DLAs searched (Table 2) used for selecting the GBT 2006 targets. These were obtained from the highest resolution radio images available, closest in frequency to the redshifted 21-cm values (ν_{θ}), although 0454+039, 0528–250 and 1418–064 have since been imaged at closer frequencies (Kanekar et al. 2009a). For the remainder of the DLA sample, refer to Curran et al. (2005, 2007b).

QSO	θ_{QSO} [arcsec]	ν_{θ} [GHz]	Reference
0454+039	<0.4	2.3	Beasley et al. (2002)
0528–250	0.010	5.0	Fomalont et al. (2000)
0758+475	0.91	1.4	FIRST
J0816+4823	0.35	1.4	FIRST
0957+561A	11.36	5.0	Harvanek et al. (1997)
1402+044	1.35	1.4	FIRST
1418–064	1.27	1.4	FIRST
2136+141	0.002	5.0	Gurvits, Kellermann & Frey (1999)

FIRST: The Very Large Array’s *Faint Images of the Radio Sky at Twenty Centimetres*.

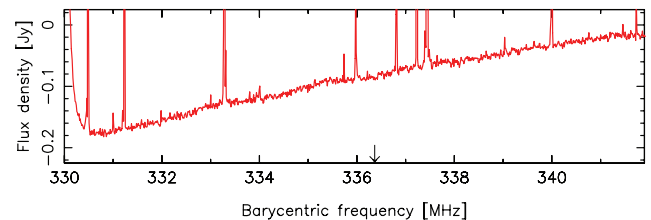


Figure 1. GBT 336 MHz band spectrum towards 0758+475 shown at a velocity resolution of 10 km s^{-1} . The arrow in this and the following spectra (Figs 2–10) indicates the expected frequency of the absorption.

cessor, using 1024 lags over a 10 MHz band, giving a channel spacing of 9.766 kHz.

0758+475 was observed on 2006 December 1 for a total of 7 h. At a central frequency of 336 MHz, the channel spacing of the GBT spectrometer gave a resolution of 0.34 km s^{-1} . The system temperature was typically $T_{\text{sys}} \approx 120 \text{ K}$ and RFI was not too severe, allowing 6.0 h of data to be retained. Although most spectral baselines were flat with the odd intermittent spike, the measured fluxes were found to vary considerably between scans (from ≈ -1 to 1 Jy), not permitting us to determine the flux density of this source (Fig. 1).

1402+044 was observed at a central frequency of 385 MHz on 2006 November 30 and December 1, for a total of 1.7 h. As per previous Westerbork Synthesis Radio Telescope observations towards this object (described in Curran et al. 2007b), the relatively wide band of the GBT spectrometer could cover the $z = 2.688$ (385.14 MHz) and 2.713 (382.55 MHz) candidate sub-DLAs of Turnshek et al. (1989), as well as the $z = 2.708$ DLA (383.07 MHz). At 385 MHz, the GBT spectrometer gives a spectral resolution of 0.30 km s^{-1} . Typically, the system temperatures were $T_{\text{sys}} \approx 110 \text{ K}$ and the removal of RFI dominated scans left a total observing time of 1.4 h (Fig. 2).

The $z = 2.485$ absorber was observed using the spectral processor, tuned to a central frequency of 408 MHz, on 2007 January 6 and 8 for a total of 7.2 h, of which 6.1 h were retained ($T_{\text{sys}} \approx 70 \text{ K}$). The channel width was 9.766 kHz, giving a spectral resolution of 7.2 km s^{-1} at 408 MHz (Fig. 3).

1418–064 was observed using the spectral processor, tuned to a central frequency of 320 MHz, on 2007 March 22 for a total

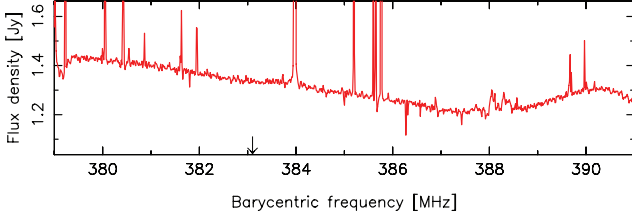


Figure 2. GBT 385 MHz band spectrum towards 1402+044 shown at a velocity resolution of 10 km s^{-1} .

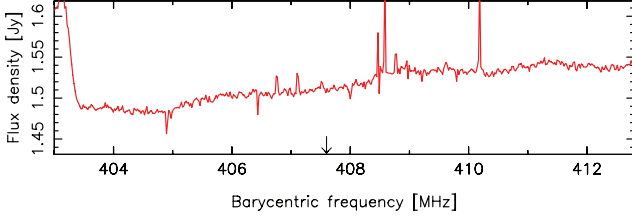


Figure 3. GBT 408 MHz band spectrum towards 1402+044 hanning smoothed to a velocity resolution of 14 km s^{-1} .

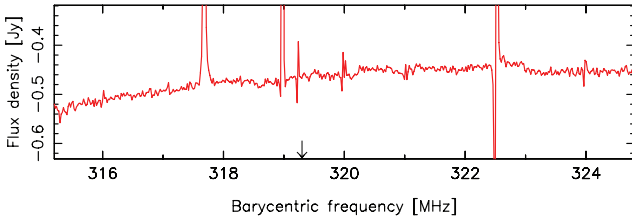


Figure 4. GBT 320 MHz band spectrum towards 1418-064 hanning smoothed to a velocity resolution of 18 km s^{-1} .

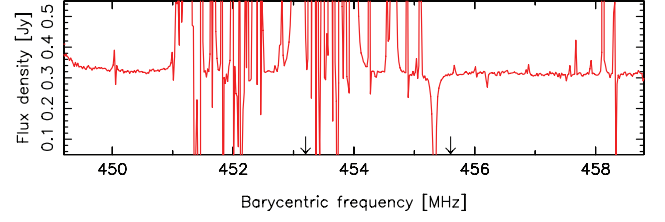


Figure 5. GBT 454 MHz band spectrum towards 2136+141 hanning smoothed to a velocity resolution of 13 km s^{-1} .

of 2.4 h, of which 1.9 were retained ($T_{\text{sys}} \approx 80 \text{ K}$). As per 0758+475, although the bandpasses were flat, the measured flux density varied considerably between scans not permitting us to determine a value for this (Fig. 4). The spectral resolution was 9.2 km s^{-1} at 319 MHz.

2136+141 was observed using the spectral processor, tuned to a central frequency of 454 MHz, on 2007 January 5 and 7. Originally, 12 h were planned to search for 21-cm absorption in the two (admittedly weak, Table 2) absorbers towards this compact quasar (Table 1), but due to severe RFI over most of this band, we only observed for 2.0 h (where $T_{\text{sys}} \approx 65 \text{ K}$). At redshifts of $z = 2.118$ and 2.134, the 10 MHz band centred on 454 MHz covered both 455.6 and 453.2 MHz at a resolution of 6.5 km s^{-1} , with the RFI dominating 451–455 MHz. This allowed us to only obtain a limit for the lower redshift sub-DLA, which itself may not be reliable (Fig. 5).

All of the data were reduced using the GBTIDL package. After flagging, both polarizations were combined, linear (first order) baselines removed and the resulting data Gaussian smoothed, via the GSMOOTH task, to a resolution of $\geq 3 \text{ km s}^{-1}$. The results are summarized in Table 2.

Table 2. Our search results. z_{abs} is the redshift of the DLA giving the observed 21-cm frequency, ν_{obs} , RUN gives the observing run (Sections 2.1–2.3), S is the flux density at ν_{obs} , σ is the rms noise level reached per $\Delta\nu$ channel (km s^{-1}), where these are $>3 \text{ km s}^{-1}$; for the GBT observations, the resolutions are typically much finer (Section 2.1). Since the measured rms noise is dependent upon the spectral resolution, as usual (Curran et al. 2005, 2007b), for the non-detections the 3σ upper limits of τ_{peak} at a velocity resolution of 3 km s^{-1} are quoted. The total neutral hydrogen column density, N_{HI} (cm^{-2}), is given with the corresponding reference, which yields the quoted spin temperature/covering factor ratio, via the estimated FWHM (km s^{-1}) for the non-detections (see main text).

QSO	z_{abs}	ν_{obs} (MHz)	RUN	S (Jy)	σ (mJy)	$\Delta\nu$	τ_{peak}	$\log_{10} N_{\text{HI}}$	Ref.	FWHM	T_{spin}/f [K]
0454+039	0.8596	763.8	GBT08	0.70	<4.6	3.0	<0.020	20.7	S95	19	>690
0528-250	2.811	372.7	GBT08	0.561	$<6.9^a$	3.0	<0.037	21.3	L96	40	>700
J0801+4725*	3.2228	336.4	GBT06	–	<6.1	3.0	–	20.7	P05	–	–
–	–	–	GMRT	0.24	<2.9	3.5	<0.039	–	–	20^\dagger	>330
J0816+4823	3.4358	320.2	GMRT	0.08	<6.3	3.7	<0.29	20.8	P05	20^\dagger	>60
0957+561A	1.391	594.0	GBT08	–	–	–	–	20.3	T93	30	–
1402+044	2.713	382.5	GBT06	1.41	<16	3.0	<0.034	–	T89	–	–
–	2.708	383.1	GBT06	1.41	<16	3.0	$<0.034^b$	20.9	P04	20^\dagger	>610
–	2.688	385.1	GBT06	1.37	$<20^c$	3.0	<0.044	–	T89	–	–
–	2.485	407.6	GBT06	1.51	<4.8	7.2	<0.015	20.2	T89	20^\dagger	>270
1418-064	3.449	319.3	GBT06	0.374 ^d	<8.1	9.2	<0.12	20.4	E01	25	>40
2136+141	2.134	453.2	GBT06	–	–	–	–	19.8	T89	–	–
–	2.118	455.6	GBT06	0.320	<7.7	6.4	<0.11	19.8	T89	20^\dagger	>10

Notes. *0758+475 – observed with both the GBT and GMRT (Sections 2.1 and 2.2). [†]No Mg II equivalent width or metallicities found, so 20 km s^{-1} assumed. ^aOver 372.53–373.20 MHz ($z = 2.8060 - 2.8132$). ^bDouble the sensitivity reached with the Westerbork Synthesis Radio Telescope observations (Curran et al. 2007b), so we adopt this limit. ^cSubject to an RFI spike from 385.17 to 385.23 MHz ($z = 2.6872 - 2.6877$). ^dFlux density could not be determined from our observations and so have adopted value for TXS 1418-064 at 0.374 Jy (Douglas et al. 1996), although this is $4' 6''$ from PKS B1418-064 (for which $S_{2.7\text{GHz}} = 0.38 \text{ Jy}$ and $S_{5.0\text{GHz}} = 0.34 \text{ Jy}$) it is within the Texas survey beam.

References: T89 – Turnshek et al. (1989), T93 – Turnshek & Bohlin (1993), S95 – Steidel et al. (1995), L96 – Lu et al. (1996), E01 – Ellison et al. (2001), P04 – Prochaska & Herbert-Fort (2004), P05 – Prochaska et al. (2005).

2.2 GMRT 2008 observations

2.2.1 Motivation

For the GMRT sample, the intent was to find new high-redshift ‘end points’ with which to verify the flattening off of T_{spin}/f at ≈ 2000 K at $z_{\text{abs}} \gtrsim 2$ (Curran et al. 2007b). To this end, we trawled the Sloan Digital Sky Survey Damped Ly α Survey Data Releases 1–3 (Prochaska et al. 2005) for DLAs occulting radio-loud quasars yet to be searched for 21-cm absorption. This yielded two DLAs occulting quasars with flux densities in excess of 50 mJy at 1.4 GHz, J080137.6+472528.2 and J081618.9+482328.4.

2.2.2 Observations and data reduction

For all of the observations, all 30 antennae were used with the 325 MHz receiver, where for an antenna gain of 0.32 Ky Jy^{-1} we expected to reach an rms of $\sigma \approx 3$ mJy per channel in each of the two polarizations. For the backend, we used a correlator bandwidth of 0.5 MHz, giving a velocity resolution of $\approx 4 \text{ km s}^{-1}$ and a coverage of $\approx \pm 230 \text{ km s}^{-1}$ ($\Delta z \approx \pm 0.003$).

J0801+472 (which is 0758+475, Section 2.1) was observed at a central frequency of 336.366 MHz on 2008 January 7 and 8. 3C 147 was used for the bandpass calibration and 0834+555 was observed every 0.6 h to correct for delays. In general, RFI was minimal and the data were excellent with all 30 antennae operating, although pairs involving antennae 13 & 28 were flagged due to poor phase stability. On the first night, the target was observed for a total of 7.54 h, of which only 0.14 h required flagging and 350 good baseline pairs were retained. On the second night, the target was observed for a total of 7.78 h of which 7.64 h were kept. Again the data were of high quality, giving 400 good baseline pairs (Fig. 6). After analyzing each polarization of each night separately, a combined image was produced using the `INVERT` task in `MIRIAD`. The source was unresolved by the $13 \times 11 \text{ arcsec}^2$ beam.

J0816+4823 was observed at a central frequency of 320.214 MHz for a total of 7.8 h on 2008 March 16. 3C 48 was used for the bandpass calibration and again the phase calibrator 0834+555 was observed every 0.6 h during the observation. After flagging the non-operating antennae, 8 and 28, as well as antenna 6, on which the phase stability was poor, RFI appeared minimal and only a little time-dependent interference had to be removed (leaving 7.65 h of data). However, perhaps due to its low flux density, an accurate image of the quasar could not be produced. We therefore flagged noisy antenna pairs until the averaged visibilities gave an rms noise level close to the ≈ 10 mJy expected. Averaging the ≈ 250 remaining baselines in each of the polarizations (Fig. 7) gave a similar flux density to extracting this from the cube, i.e. 85 mJy at 0.32 MHz, which compares well with the 78 mJy at 1.4 GHz from The Very Large Array’s Faint Images of the Radio Sky at Twenty Centimetres (FIRST). Again, the results are summarized in Table 2.

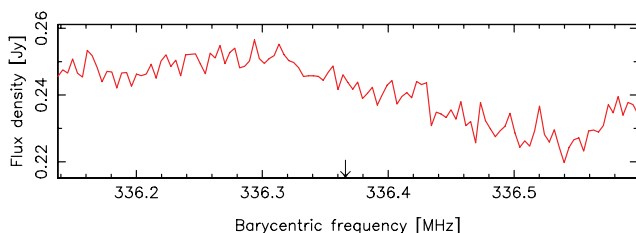


Figure 6. GMRT 336 MHz band spectrum towards J0801+472 (0758+475). The velocity resolution is 3.5 km s^{-1} .

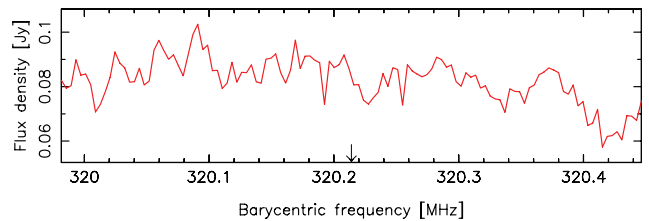


Figure 7. GMRT 320 MHz band spectrum towards J0816+4823. The velocity resolution is 3.7 km s^{-1} .

2.3 GBT 2008 observations

2.3.1 Motivation

According to the 21-cm line strength–metallicity correlation (T_{spin}/f –[M/H] anticorrelation; Curran et al. 2007b), there are three previously searched DLAs (PKS 0454+039, PKS 0528–250 and [HB89] 0957+561) for which the spin temperature/covering factor ratio should be $T_{\text{spin}}/f \lesssim 1000$ K, with the previous limits possibly being close to those required to detect 21-cm absorption. We therefore applied for GBT time in order to improve these limits to the point where 21-cm absorption would be detected, although a significant improvement was only managed for 0528–250 (see Sections 3.1 and 4.2).

2.3.2 Observations and data reduction

As per the 2006 run, we used the GBT Prime Focus Receivers in position switching mode, with the GBT spectrometer split into 32 768 lags over a 12.5 MHz band, giving a channel spacing of 763 Hz, in dual polarization.

0454+039 was observed for a total of 2.9 h over several runs from 2008 August 28 to September 13, at a central frequency of 763.8 MHz, giving a spectral resolution of 0.3 km s^{-1} . System temperatures ranged from $T_{\text{sys}} \approx 30$ –40 K over these dates and the overall RFI was minimal, except over the frequency range of interest, 763.6 to 763.8 MHz, where a blooming great spike appeared in most of the spectra. This led to significant flagging, leaving 1.2 h of good data, of which the average spectrum is shown in Fig. 8.

0528–250 was observed on 2008 February 2 and 18 for a total of 7.4 h, at a central frequency of 327.7 MHz, giving a spectral resolution of 0.7 km s^{-1} . The system temperature was typically $T_{\text{sys}} \approx 60$ K and RFI was only severe over 0.64 h of the observations. However, besides this there were intermittent RFI spikes over the whole band, which only permit rms estimates over the intervening clean regions. Therefore, the limit quoted in Table 2 is for 372.53 to 373.20 MHz ($z = 2.8060$ – 2.8116), close to that expected from the redshift of the DLA (Fig. 9).

0957+561A was observed for a total of 3.6 h over several runs from 2008 August 7 to November 8, at a central frequency of

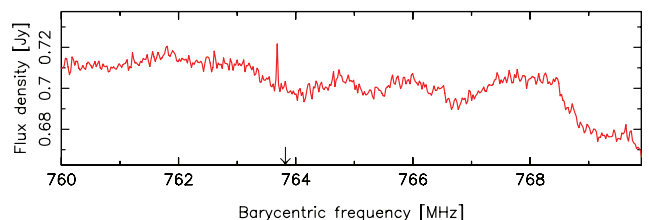


Figure 8. GBT spectrum towards 0454+039, shown at a velocity resolution of 10 km s^{-1} .

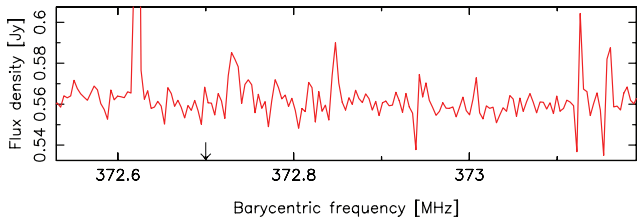


Figure 9. GBT spectrum towards 0528–250 over the relatively RFI free 372.53–373.20 MHz, shown at a velocity resolution of 3 km s^{-1} .

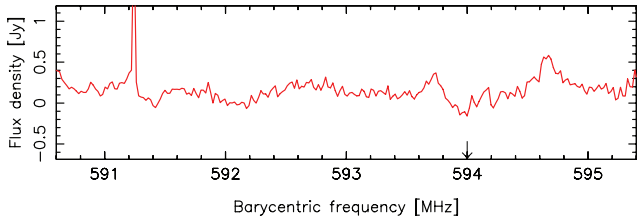


Figure 10. GBT spectrum towards 0957+561A over the relatively RFI free 590.6–595.4 MHz, shown at a velocity resolution of 10 km s^{-1} .

594 MHz, giving a spectral resolution of 0.4 km s^{-1} . System temperatures ranged from $T_{\text{sys}} \approx 30$ to 60 K over these dates and RFI was severe. This led to extensive flagging of bad data, leaving only 14 min of ‘good data’, of which the average spectrum is shown in Fig. 10. Although this flagging removed all of the spikes close to 594 MHz, a strong ringing was still present in the unsmoothed data and, as seen from the spectrum, no reasonable limit can be obtained from these observations.¹

3 RESULTS

3.1 Observational results

Typically, the illumination of the optical (Lyman α) and radio (21-cm) absorbers arise from quite different sources sizes, these being $\lesssim 1 \text{ pc}$ for the former, but in excess of 100 pc for the latter² (Wolfe, Gawiser & Prochaska 2005 and references therein). Thus, it is possible that the optical and radio observations could trace different sight lines (as is probably the case for 1622+238; Curran et al. 2007a). However, if the 21-cm and Lyman α absorption do arise in the same cloud complexes (Dickey & Lockman 1990), the column density (cm^{-2}) of the absorbing gas in a homogeneous cloud is related to the velocity integrated optical depth, where $\tau \equiv -\ln(1 - \frac{\sigma}{fS})$, of the 21-cm line via (Wolfe & Burbidge 1975)

$$N_{\text{HI}} = 1.823 \times 10^{18} T_{\text{spin}} \int \tau \, dv, \quad (1)$$

where T_{spin} (K) is the mean harmonic spin temperature of the gas, σ the depth of the line (or rms noise in the case of a non-detection) and S and f the flux density and covering factor of the background continuum source, respectively. In the optically thin regime ($\sigma \ll f \cdot S$), equation (1) reduces to $N_{\text{HI}} = 1.823 \times 10^{18} \frac{T_{\text{spin}}}{f} \int \frac{\sigma}{S} \, dv$, which we apply to the entries in Table 2, where we summarize the results for the three sets of observations.

¹ Note that the unflagged data give a flux density of $\approx 1 \text{ Jy}$, although the spectrum is plagued by RFI spikes close to the target frequency.

² Even over 10 kpc in some cases (see fig. 4 of Curran et al. 2005).

For our and the previous non-detections, we have no knowledge of what the full width at half-maximum (FWHM) of the 21-cm profile should be, thus hampering the determination of a lower limit for T_{spin}/f . Previously (Curran et al. 2005, 2007b), we have used the $\approx 20 \text{ km s}^{-1}$ mean of the detections to derive velocity integrated optical depth limits for the non-detections. An alternative to this is to estimate the FWHMs from the spin temperature, via the kinetic temperature according to $T_{\text{spin}} \approx T_{\text{kin}} \lesssim 22 \times \text{FWHM}^2$ (e.g. Kanekar & Chengalur 2003), although in the absence of detailed knowledge of the covering factor, it is impossible to assign a specific spin temperature to any of the DLAs. In light of the findings of Curran et al. (2007b), however, we can make educated guesses to the profile widths according to the FWHM–Mg II rest-frame equivalent width correlation for the detections. This gives $\text{FWHM} \approx 13 W_{\text{r}}^{\lambda 2796}$ (fig. 6 of Curran et al. 2007b), and, where the Mg II equivalent widths are not available (generally at $z_{\text{abs}} \gtrsim 2.2$), we estimate these from the metallicity via $W_{\text{r}}^{\lambda 2796} \approx 2.0 [\text{M}/\text{H}] + 4.0$ (fig. 7 of Curran et al. 2007b; see also Murphy et al. 2007).³ Note that, although Gupta et al. (2009) and Kanekar et al. (2009b) find that the FWHM– $W_{\text{r}}^{\lambda 2796}$ correlation does not generally hold for Mg II absorption systems, when only those which are likely to be DLAs (i.e. with an Mg I 2852 Å equivalent width of $W_{\text{r}}^{\lambda 2852} > 0.5 \text{ Å}$; Rao, Turnshek & Nestor 2006) are added to the sample, the correlation is still found to hold for all suspected DLAs (Curran 2009).

Commenting on our observational results, due to the effects of RFI and weak radio fluxes, we cannot assign limits to four of the absorbers and the limits for a further three are so poor as to be of little use. Of the remaining five, for 0454+039 we have matched the previous limit of $T_{\text{spin}}/f \gtrsim 600 \text{ K}$ (Briggs & Wolfe 1983), while for 0528–250 we have significantly improved upon the $T_{\text{spin}}/f \gtrsim 100 \text{ K}$ limit of Carilli et al. (1996).⁴ This is the first search for 21-cm absorption at $z_{\text{abs}} = 3.223$ towards J0801+4725, although, due to the relatively low flux density, the limit is only $T_{\text{spin}}/f \gtrsim 300 \text{ K}$.⁵ For the $z_{\text{abs}} = 2.708$ DLA towards 1402+044, we have improved the previous limit (Curran et al. 2007b) by a factor of 2 and for the $z_{\text{abs}} = 2.485$ sub-DLA, publish the first limit, although this is weak due to the low neutral hydrogen column density.

3.2 Update of the previous results

Adding the new results and applying the estimated FWHMs, in Fig. 11 we update the spin temperature/covering factor–absorption redshift distribution of Curran et al. (2005). From the histogram, it is seen that the low-redshift absorbers have a similar T_{spin}/f distribution to those at high redshift ($z_{\text{abs}} \geq 1.6$) and in Table 3 we present the results of the statistical tests performed on the low- and high-redshift samples. These were done for redshift cuts of $z_{\text{CUT}} = 1.0, 1.6$ (the turnover in angular diameter distance, Section 4.1.1) and 2.0 (as Kanekar & Chengalur 2003). From these, we find slightly lower mean values of T_{spin}/f for the low-redshift

³ Applying the above conversions gives a range of $5\text{--}42 \text{ km s}^{-1}$ for the non-detections, thus not drastically changing the values of $\log_{10}(T_{\text{spin}}/f)$, shown in the following figures, from those using a FWHM of 20 km s^{-1} .

⁴ Based upon our 3 km s^{-1} resolution and 40 km s^{-1} linewidth (Table 2).

⁵ For this and the other GMRT target, J0816+4823, it is possible that the redshift coverage of $z_{\text{abs}} \pm 0.003$ is not sufficient to cover uncertainties in the absorber redshift, which are determined from the Lyman α line (Prochaska et al. 2005). However, J0801+4725 has been searched over $z_{\text{abs}} = 3.30 \pm 0.08$ with the GBT (Fig. 1) and the J0816+4823 T_{spin}/f limit is too poor in any case to contribute to the analysis.

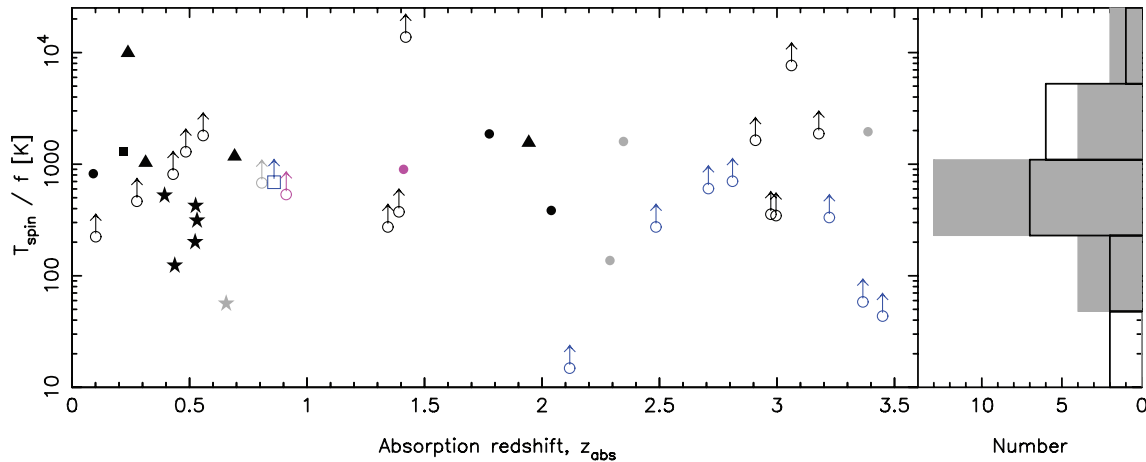


Figure 11. The spin temperature/covering factor ratio versus the absorption redshift for the DLAs searched in 21-cm absorption. The shapes represent the type of galaxy with which the DLA is associated: circle – unknown type, star – spiral, square – dwarf, triangle – low surface brightness. The filled symbols represent the 21-cm detections and the unfilled symbols+arrows show the lower limits for the non-detections (all of these bar one, 0454+039 at $z_{\text{abs}} = 0.8596$, have unknown host identifications). The grey symbols show the results since Curran et al. (2005) and the coloured symbols show the new results presented here (blue) as well as those of Kanekar et al. (2009b) (magenta). The solid grey histogram shows the spin temperature/covering factor distribution for the low-redshift ($z_{\text{abs}} < 1.6$) absorbers and the outlined histogram the distribution for the high-redshift ($z_{\text{abs}} \geq 1.6$) absorbers, where the limits to T_{spin}/f are treated as detections.

Table 3. The statistics for and between the low- and high-redshift samples for various redshift cuts, where P gives the probability that the low- and high-redshift DLAs are drawn from the same sample and S gives the corresponding significance (assuming Gaussian statistics). The values in the first four rows incorporate the limits to the non-detections via the `ASURV` package (Isobe et al. 1986) and for the Kolmogorov–Smirnov test the limits are treated as detections (as per Kanekar & Chengalur 2003).

	$z_{\text{CUT}} = 1.0$		$z_{\text{CUT}} = 1.6$		$z_{\text{CUT}} = 2.0$	
	$z_{\text{abs}} < z_{\text{CUT}}$	$z_{\text{abs}} \geq z_{\text{CUT}}$	$z_{\text{abs}} < z_{\text{CUT}}$	$z_{\text{abs}} \geq z_{\text{CUT}}$	$z_{\text{abs}} < z_{\text{CUT}}$	$z_{\text{abs}} \geq z_{\text{CUT}}$
Sample size, n	19	20	23	18	25	16
Mean, $\log_{10}(T_{\text{spin}}/f)$	3.08 ± 0.18	3.38 ± 0.18	3.16 ± 0.17	3.26 ± 0.16	3.11 ± 0.15	3.30 ± 0.20
$P_{\text{log-rank}}$		0.0718		0.265		0.203
$S_{\text{log-rank}}$		1.80σ		1.39σ		1.27σ
P_{KS}		0.443		0.448		0.358
S_{KS}		0.767σ		0.759σ		0.919σ

absorbers, with log-rank and Kolmogorov–Smirnov tests indicating that there is little significance in the differences between the low- and high-redshift samples. Bear in mind, however, that the FWHMs for the non-detections have been estimated (Section 3.1), with some of these relying on a secondary correlation ($\text{FWHM} \propto W_r^{\lambda 2.796} \approx 2.0 [\text{M}/\text{H}] + 4.0$), when the Mg II equivalent width is not available.⁶ Furthermore, the Kolmogorov–Smirnov test treats the upper limits as actual values and higher sensitivity limits at high redshift are required in order to confirm the similarities between the samples apparent in Table 3.

Performing a Kolmogorov–Smirnov test on the redshift distributions between the detections and non-detections, thus requiring no assumptions, gives an 11 per cent probability (significant at 1.6σ) that these are drawn from the same sample. Additionally, the non-detections have a higher mean redshift – $\bar{z}_{\text{abs}} = 1.77(\sigma = 1.08)$, compared to $\bar{z}_{\text{abs}} = 1.13(\sigma = 0.96)$ for the detections. Therefore, we cannot rule out that the

T_{spin}/f distribution differs between the two redshift regimes. Although the relative contributions of T_{spin} and f are unknown, the fact that the largest differences are seen for $z_{\text{CUT}} = 1.0$ (where $[T_{\text{spin}}/f]_{z < 1} = 1200 \text{ K}$ cf. $[T_{\text{spin}}/f]_{z \geq 1} = 2400 \text{ K}$) is consistent with geometry effects giving larger values of f at $z_{\text{abs}} < 1$ (Curran & Webb 2006 and Section 4.1.1).

While we are discussing statistical trends over the whole sample, it should be emphasized that the 21-cm absorption searches yield a very heterogeneous sample, with each survey having different selection criteria (including the three here), resulting in a mix of detections and non-detections across various absorber morphologies (where these are known, Fig. 11). However, presuming that the optical and radio absorption clouds are coincident, equation (1) accounts for differences in the neutral hydrogen column densities and the flux densities of the background sources (discussed in detail in Curran et al. 2005), leaving only the T_{spin}/f degeneracy. Naturally, various properties of the absorber and emitter, as well as the distance between them, could influence this ratio, issues which we discuss here. However, whether it be due to similar values of T_{spin} and f for all of the absorbers, or just the ratio being maintained, there may be no large differences between the low- and high-redshift samples. Furthermore, since $f \leq 1$, the ordinate in Fig. 11 represents the maximum possible spin temperatures for the detections of which

⁶ Setting the FWHMs obtained from the metallicity to 20 km s^{-1} , however, alters only the $z_{\text{abs}} \geq z_{\text{CUT}}$ averages in Table 3, and these only slightly. Overall, there is very little change with $S_{\text{log-rank}} = 1.95, 1.45$ and 1.45σ and $S_{\text{KS}} = 1.15, 1.22$ and 0.42σ , respectively.

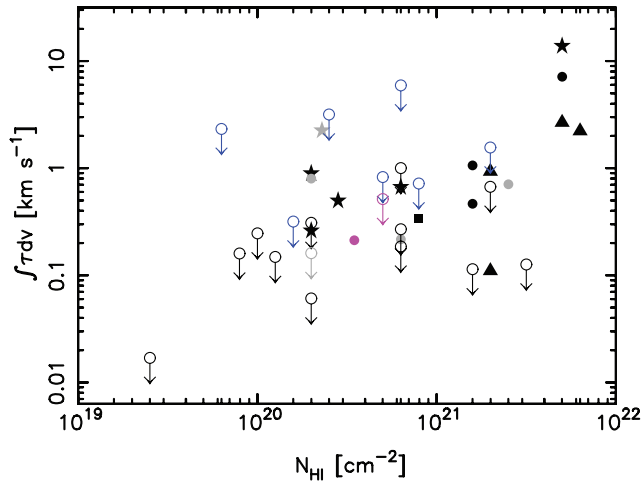


Figure 12. The velocity integrated optical depth of the 21-cm absorption versus the total neutral hydrogen column density. The symbols are as per Fig. 11.

there are now several at $z_{\text{abs}} \gtrsim 2$. This indicates that high redshifts do not *necessarily* entail high spin temperatures, as advocated by Kanekar & Chengalur (2003) [although a larger fraction of warm gas (Kanekar et al. 2009a) does not exclude the possibility of cold clumps]. Case in points against exclusively high spin temperatures at high redshift are:

- (i) The 21-cm detection at $z_{\text{abs}} = 2.289$ towards 0311+430 (York et al. 2007), which has one of the lowest ‘spin temperatures’ yet found, i.e. $T_{\text{spin}}/(f = 1) \approx 140$ K.
- (ii) The excitation temperature of $T_{\text{ex}} \approx 50$ K derived from the H_2 transitions in the $z_{\text{abs}} = 2.626$ DLA towards 0812+32B, indicating the presence of cold gas (Jorgenson et al. 2009).
- (iii) The other 17 DLAs in which H_2 has been detected (Noterdaeme et al. 2008 and references therein). These are generally at $z_{\text{abs}} \gtrsim 1.7$, although they may represent a specific class of absorber within the general DLA population (Curran et al. 2004; Murphy, Curran & Webb 2004).

Lastly, Curran et al. (2005) also noted a correlation between the integrated 21-cm optical depth and the H I column density. Updating this for the DLAs (Fig. 12) and incorporating the upper limits (as above), there is a probability of $P(\tau) = 0.0021$ that the correlation occurs by chance. This corresponds to a 3.08σ significance and, since the gradient is $\propto f/T_{\text{spin}}$, suggests that, on the whole, the ratio of spin temperature to covering factor is a constant for DLAs, although there is some considerable scatter.

4 DISCUSSION

4.1 Covering factors

4.1.1 Angular diameter distances and other effects

As mentioned in Section 2.1, Curran et al. (2005) suggested that, contrary to the high redshift equals high spin temperature argument of Kanekar & Chengalur (2003), 21-cm absorption should be readily detectable at high redshift towards compact radio sources, where the covering factor is maximized. At the time of writing up the results presented in Curran & Webb (2006), this was confirmed by the detection of 21-cm absorption in the highest redshift example to date, at $z_{\text{abs}} = 2.347$ towards 0438–436 (Kanekar et al. 2006),

which has a background radio source size of only 0.039 arcsec at 5 GHz (Tingay et al. 1998). Following this, since submitting the proposal for the 2006 GBT observations, 21-cm absorption has been confirmed at yet higher redshift, $z_{\text{abs}} = 3.386$ towards 0201+113 (Kanekar et al. 2007; see also de Bruyn, O’Dea & Baum 1996; Briggs, Brinks & Wolfe 1997), as well as at $z_{\text{abs}} = 2.289$ towards 0311+430 (York et al. 2007). Again, both of these occult compact radio sources of < 0.007 arcsec at 1.4 GHz (Stanghellini et al. 1990)⁷ and 1.36×0.63 arcsec², respectively. The latter was noted by York et al. (2007) to be unusual in its low spin temperature of $T_{\text{spin}} \leq 140$ K at such a high redshift, although this is not unusual in regard to the finding of Curran et al. (2005) and Curran & Webb (2006).

From Table 1, we see that five of our targets are towards radio source sizes of $\theta_{\text{QSO}} \lesssim 1$ arcsec (recently found to be 0.07 arcsec for 0454+039 and 0.17 arcsec for 0528–250; Kanekar et al. 2009a), although we have only meaningful T_{spin}/f limits for three of these (0454+039, 0528–250 and 0758+475 – Table 2). However, all of the GBT 2006 targets (Section 2.1) were selected before the arguments of Curran & Webb (2006) were formulated, and so all of the 2006 targets (and two of the three just mentioned) are all at high redshift, and will therefore be disadvantaged with respect to the DLA to QSO angular diameter distance ratios.

Showing these in Fig. 13 (top panel), we see that all but one of our target DLAs (for which we have limits) are indeed at angular diameter distance ratios of $\text{DA}_{\text{DLA}}/\text{DA}_{\text{QSO}} \approx 1$, due to their high-redshift selection. For a given absorber and radio source size, this will disadvantage the effective covering factor (possibly giving the observed $\overline{[T_{\text{spin}}/f]_{z \geq 1}} \approx 2 \overline{[T_{\text{spin}}/f]_{z < 1}}$, Section 3.2), although, as mentioned above, the three new high-redshift detections occult compact radio sources, as shown in the bottom panel of Fig. 13, where we use the source sizes compiled in Curran et al. (2005) updated with those given in Kanekar et al. (2009a).⁸ However, all of our non-detections (which are predominately at $z_{\text{abs}} \gtrsim 2.4$) also occult similar radio source sizes. Of these, three of the sizes are not as reliable (orange symbols where $3 < \nu_{\text{size}}/\nu_{\text{abs}} < 10$, cf. green where $\nu_{\text{size}}/\nu_{\text{abs}} \leq 3$), although as seen from Fig. 11, only three published non-detections are sufficiently sensitive to detect $T_{\text{spin}}/f \gtrsim 2000$ K at $z_{\text{abs}} \gtrsim 2$ (Section 2.2).

While, due to geometry effects, a high angular diameter distance will disadvantage the absorption cross-section in comparison to the same absorber placed at a low angular diameter distance, with the 21-cm searches spanning a look-back time range of 12 Gyr, there are also evolutionary effects to be considered. For instance, an evolution in the morphologies of the absorbing galaxies is expected to result in different metallicities and these heavy elements can provide cooling pathways for the diffuse gas (Dalgarno & McCray 1972). Furthermore, it is shown that the relative mix of the cold

⁷ Kanekar et al. (2007) report a deconvolved source size of 17.6×6.6 mas² at 328 MHz.

⁸ Many of the source sizes are measured at very long baseline interferometry frequencies, which are often many times higher than that of the redshifted 21-cm line (see table 2 of Curran et al. 2005), and so in Fig. 13 (bottom panel) we have flagged each of the DLAs according to how many times larger than $1420/(z_{\text{abs}} + 1)$ the frequency at which the source size is measured, i.e. $\nu_{\text{size}}/\nu_{\text{abs}}$. The recently published low-frequency Very Long Baseline Array imaging of Kanekar et al. (2009a) accounts for many of the ‘green’ values, where $\nu_{\text{size}}/\nu_{\text{abs}} \leq 3$. Since a number of these sources appear resolved, we have recalculated the extents, rather than using the deconvolved sizes quoted in Kanekar et al. (2009a), which are often smaller than the beam and may be unphysical (e.g. ~ 0 pc for 0405–331).

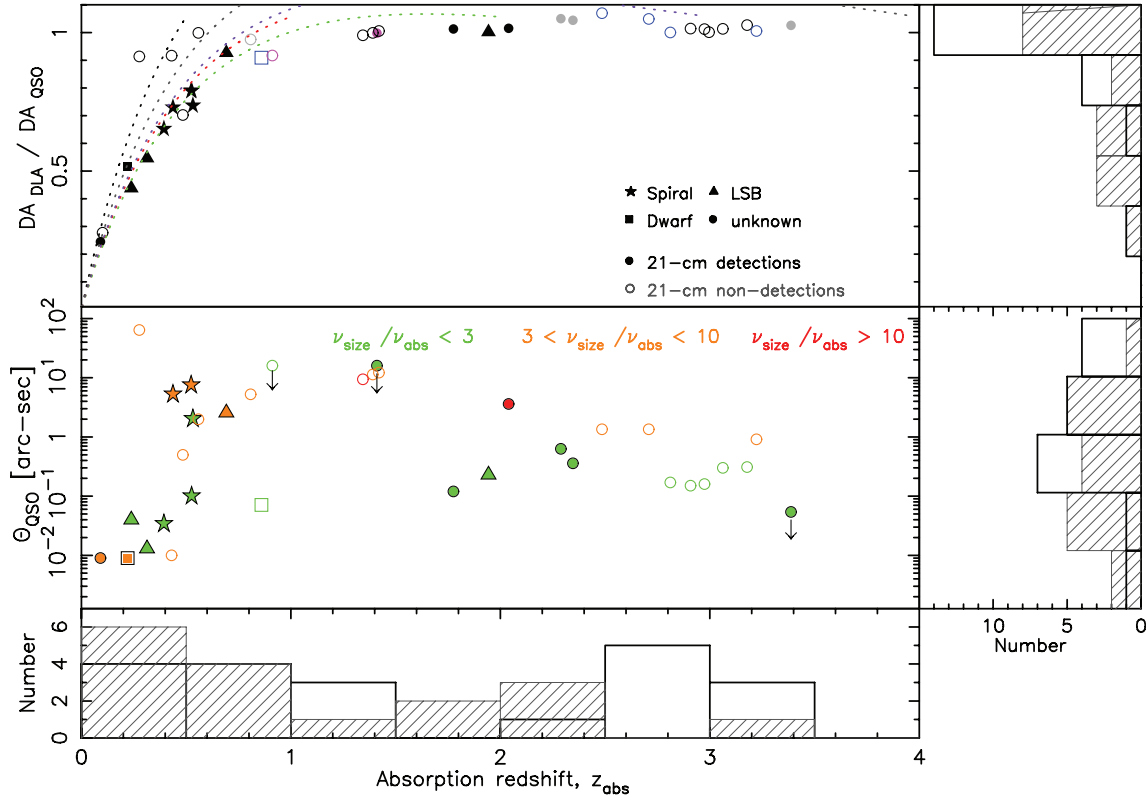


Figure 13. Top: The absorber/quasar angular diameter distance ratio versus the absorption redshift. Updated from Curran & Webb (2006), where the symbols are as per Fig. 11 and we include only the DLAs which have been searched to $T_{\text{spin}}/f \geq 100$ K (see main text). The iso-redshift curves show how $DA_{\text{DLA}}/DA_{\text{QSO}}$ varies with absorption redshift, where DA_{QSO} is for a given QSO redshift, given by the terminating value of z_{abs} (throughout this paper, we use $H_0 = 71$ $\text{km s}^{-1} \text{Mpc}^{-1}$, $\Omega_{\text{matter}} = 0.27$ and $\Omega_{\Lambda} = 0.73$). That is, we show the $DA_{\text{DLA}}/DA_{\text{QSO}}$ curves for $z_{\text{em}} = 0.5, 1, 2, 3$ and 4 . Bottom: The radio source size versus the absorption redshift. The symbols are colour coded according to the ratio of the frequency of the image to the redshifted 1420 MHz frequency: green – $\nu_{\text{size}}/\nu_{\text{abs}} \leq 3$, orange – $3 < \nu_{\text{size}}/\nu_{\text{abs}} \leq 10$ and red – $\nu_{\text{size}}/\nu_{\text{abs}} > 10$. The hatched histogram represents the detections and the bold histogram the non-detections.

neutral medium (CNM; where $T \sim 150$ K and $n \sim 10 \text{ cm}^{-3}$) and the warm neutral medium (WNM; $T \sim 8000$ K and $n \sim 0.2 \text{ cm}^{-3}$) can be affected by the metallicity (Wolfire et al. 1995).

At low redshifts, where the DLA hosts can be imaged directly, the absorbing galaxies appear to be a mix of spirals, dwarf and low surface brightness galaxies (e.g. Le Brun et al. 1997; Chen & Lanzetta 2003; Rao et al. 2003) and, in general, large galaxies appear to be more populous at low redshift with smaller morphologies becoming more common at high redshifts (Baker et al. 2000; Lanfranchi & Friaça 2003). Therefore, in the more compact absorbing galaxies, where the metallicities are lower than in the larger spirals (see Section 4.2), we may expect the gas to be more dominated by the WNM and, as shown by Curran et al. (2007b), T_{spin}/f is anticorrelated with the metallicity (see Section 4.2). However, although the metallicity is itself anticorrelated with the look-back time (Prochaska et al. 2003; Rao et al. 2005), no $[M/H]-z_{\text{abs}}$ correlation is seen for the 21-cm searched sample (Curran et al. 2007b), and, as seen in Fig. 13, very few morphologies are known for these at $z_{\text{abs}} \gtrsim 1$. Furthermore, the $T_{\text{spin}}/f-[M/H]$ anticorrelation is consistent with *either* the spin temperature being lower or the covering factor being larger at high metallicities, with the larger galaxies likely to have high values of f as well as $[M/H]$. Although the T_{spin}/f degeneracy is unbreakable, it is possible that both factors contribute and that the values of $[M/H]$, T_{spin} and f are in fact interwoven (Curran et al. 2007b).

In addition to decreasing metallicities, the increase in the background ultraviolet flux will increase the ionization fraction of the gas (Bajtlik, Duncan & Ostriker 1988), in addition to raising its spin temperature (Field 1959; Bahcall & Ekers 1969), an effect also seen in associated systems, where 21-cm absorption has never also been detected in the host galaxy of a quasar with $L_{\text{UV}} \gtrsim 10^{23} \text{ WHz}^{-1}$ (Curran et al. 2008). Therefore, as well as always having large angular diameter distance ratios and lower metallicities, high-redshift absorption systems will generally be subject to higher ultraviolet fluxes, although for intervening absorbers the effect will not be as severe as for associated absorbers. Nevertheless, this could be the cause of many of the T_{spin}/f lower limits at $z_{\text{abs}} \gtrsim 2.5$ (Fig. 11), although, again, such heated gas could have a significantly lower 21-cm absorption cross-section as well as a higher temperature.

4.1.2 Absorber extents

In order to consider the radio source size in conjunction with the ratio of the angular diameter distances, we calculate the extent of absorber required to fully cover the radio source (Fig. 14) and show this against the normalized line strength, $1.823 \times 10^{18} \int \tau dv / N_{\text{H I}} = f/T_{\text{spin}}$ (Fig. 15). From this, we see a correlation between the extent of the absorber and the 21-cm absorption strength for the detections. For the 18 detections, this is significant at 2.7σ , falling

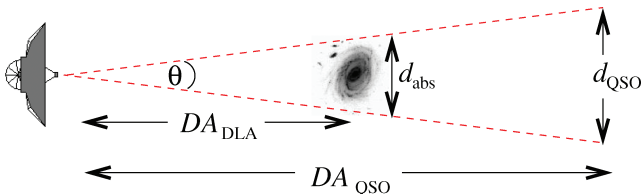


Figure 14. In the small angle approximation $\theta = d_{\text{abs}}/DA_{\text{DLA}} = d_{\text{abs}}/DA_{\text{QSO}}$, giving $d_{\text{abs}(\text{min})} = \theta_{\text{QSO}} \cdot DA_{\text{DLA}}$ when the absorber just covers the background radio source size.

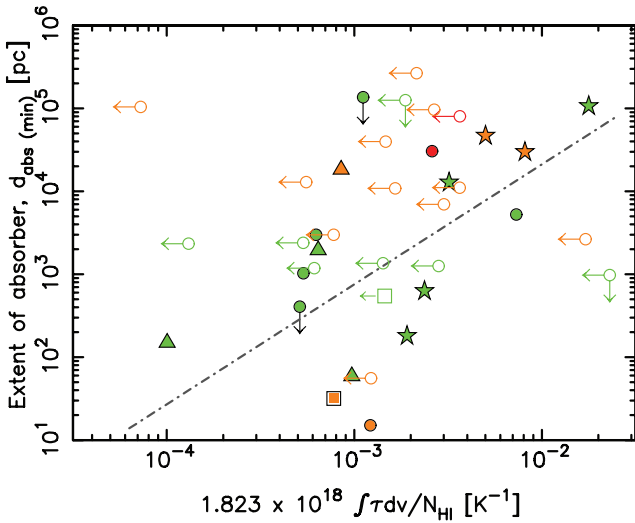


Figure 15. The minimum extent of the absorber required to cover the radio source versus the normalized line strength. The symbols are as per Fig. 13 (bottom panel). The line shows the least-squares fit to the detections. The upper limits in the ordinate are due to upper limits in the background radio source sizes.

to 2.2σ for the 12 detections with $\nu_{\text{size}}/\nu_{\text{abs}} \leq 3$ (‘green’), with the non-detections exhibiting no correlation whatsoever (bringing the significance for the whole 39 strong sample down to 1.4σ).⁹ The fit in Fig. 15 suggests that the non-detections which have been searched sufficiently deeply (i.e. neglecting the two with $f/T_{\text{spin}} \gtrsim 0.01$) may require large absorbers ($\gtrsim 10$ kpc scales) in order to achieve effective covering factors. As is seen from the figure, several detections also occupy this regime, although these tend to be spiral galaxies. Therefore, like Kanekar & Chengalur (2003), and as discussed in Curran et al. (2005), the majority of non-detections (which are at high redshift and have unknown morphologies) may be non-spirals. Although, unlike Kanekar & Chengalur (2003), we again suggest that may be their small sizes, in addition to/rather than high mean spin temperatures, which may be responsible for their weak line strengths.

⁹ Using the deconvolved values of Kanekar et al. (2009a), rather than those measured (see footnote 8), gives 2.5, 1.9 and 1.3σ , respectively.

The covering factor can be defined¹⁰ as $f \equiv [d_{\text{abs}}/(\theta_{\text{QSO}} DA_{\text{DLA}})]^2$ (Curran & Webb 2006), meaning that, in general¹¹, the ordinate in Fig. 15 is equivalent to d_{abs}/\sqrt{f} . This therefore suggests, at least for the detections, that the line strength increases with the size of the 21-cm absorption region, a trend which is apparent, even when the absorber size is weighed down by the \sqrt{f} factor and, in general, from the normalized line strength,

$$1.823 \times 10^{18} \frac{\int \tau dv}{N_{\text{HI}}} = \frac{f}{T_{\text{spin}}} \propto \theta_{\text{QSO}} DA_{\text{DLA}} = \frac{d_{\text{abs}}}{\sqrt{f}}. \quad (2)$$

That is, $d_{\text{abs}} \propto f^{3/2}/T_{\text{spin}}$, which makes sense in terms of both covering factor and spin temperature – a larger absorber implies a larger covering factor, as well as the possibility of a lower spin temperature. Presuming that this is not dominated by the numerator, this *could* suggest that the larger absorbing galaxies are subject to lower spin temperatures (Kanekar & Chengalur 2003 and references therein). However, one interpretation of the distribution of the non-detections along the ordinate in Fig. 15 is that for a given absorption cross-section (i.e. assuming the same d_{abs} for all the DLAs), the covering factor is generally lower than for a number of the detections.

Note that, in addition to geometry effects, it is possible that these lower covering factors could also be caused by lower beam filling factors, introduced by structure (‘clumpiness’) in the absorbing gas, which may be behind the 21-cm variability seen at $z_{\text{abs}} = 0.313$ towards 1127–145 (Kanekar & Chengalur 2001) and at $z_{\text{abs}} = 3.386$ towards 0201+113 (de Bruyn et al. 1996; Briggs et al. 1997; Kanekar et al. 2007). Gupta et al. (2009) also note from their large survey of Mg II absorption systems that the decreasing number density of 21-cm absorbers with redshift runs counter to that of the Lyman α and $W_r^{\lambda 2796} > 1 \text{ \AA}$ Mg II absorbers (Rao et al. 2006). This is attributed to a significant evolution in either the CNM filling factor or the covering factor, the former of which could be the result of a relatively extensive WNM, thus indicating a higher mean harmonic spin temperature (Kanekar et al. 2009a), although the larger fractions of warm gas would not exclude the presence of cold clumps. Either or both of these scenarios would be tied up in the T_{spin}/f degeneracy. Nevertheless, 21-cm detection rates are significantly lower at high redshift and the filling factor of the CNM, through either its effect on T_{spin} or f , could be a major contributor to this.

4.2 21-cm line strength–metallicity correlation

Addressing the 21-cm line strength–metallicity correlation (T_{spin}/f –[M/H] anticorrelation) of Curran et al. (2007b), the focus of the 2008 GBT observations (Section 2.3), it appears that we should have detected absorption in at least one of the two DLAs for which reasonable sensitivities were reached (Fig. 16). Regarding the best improved limit,¹² 21-cm absorption may not have been

¹⁰ It can also be estimated as the ratio of the compact unresolved component’s flux to the total radio flux (Briggs & Wolfe 1983; Kanekar et al. 2009a). However, even if high-resolution radio images at the redshifted 21-cm frequencies are available, this method gives no information on the extent of the absorber (or how well it covers the emission). Furthermore, the high angular resolution images are of the continuum only and so do not give any information about the depth of the line when the extended continuum emission is resolved out.

¹¹ That is, where d_{abs} is the actual extent of the absorber, rather than the extent minimum required to cover θ_{QSO} .

¹² By a factor of ≈ 7 , cf. Carilli et al. 1996. See footnote 4.

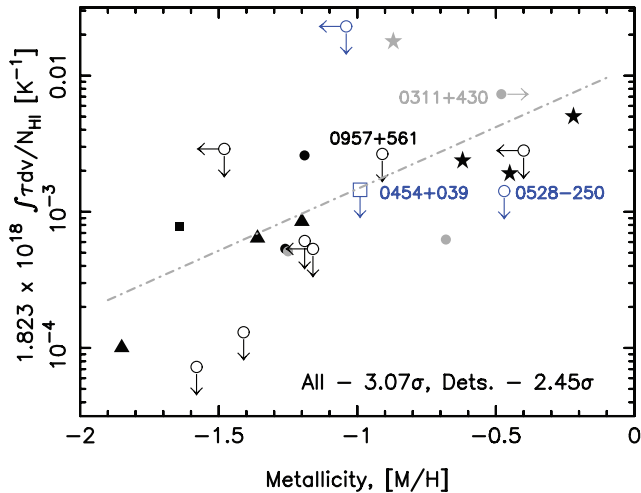


Figure 16. The normalized line strength ($\equiv f/T_{\text{spin}}$) versus the metallicity for the DLAs searched in 21-cm absorption, where the symbols are as per Fig. 11. The significance of the correlation is given for both the whole sample and the detections only and the least-squares fit for the detections shown.

detected towards 0528–250, on the grounds that, with an absorption redshift very close to that of the emission redshift (both at $z = 2.8110$; Möller, Fynbo & Fall 2004 and references therein), the absorber is possibly located in the host of the background quasar. We may therefore expect the neutral gas to be subject to excitation effects seen in other high-redshift 21-cm absorption searches (Curran et al. 2008). However, the presence of H_2 in the absorber suggests that the gas is relatively cool with $T_{\text{kin}} \approx 110\text{--}150$ K (Srianand et al. 2005) and so this is unlikely.

In any case, referring to Fig. 16, the limit is not overly low in comparison to 0438–436 [the detection at $[\text{M}/\text{H}] = -0.68$, $f/T_{\text{spin}} = 6.3 \times 10^{-4}$ (K^{-1})] and there is also the possibility that we have missed the line, with our limit only being good over the redshift range $z \approx 2.806\text{--}2.812$ (Section 2.3). Assuming this limit is reliable and including 0311+430, strengthens the correlation (cf. Curran et al. 2007b).

York et al. (2007) comment that the $z_{\text{abs}} = 2.289$ absorber towards 0311+430 has an unusually high metallicity, although according to Fig. 16, this has some leeway before the metallicity becomes atypically high. From its grouping in the line strength–metallicity plot, we suggest that the absorption is due to a spiral galaxy, as do York et al. (2007) on the basis of its low ‘spin temperature’. Support for this assertion is given by its grouping with the spirals in Fig. 15 (the ‘unknown’ at 7×10^{-3} K^{-1} , 5 kpc), although this is on the grounds of a large absorption cross-section, rather than the spin temperature.

5 SUMMARY

Through three sets of separate observations, we have undertaken a survey for 21-cm absorption in a total of 12 DLAs and sub-DLAs. Due to RFI and low neutral hydrogen column densities, useful sensitivities were obtained for five of the sample, none of which resulted in a detection. We add these to the recent results from other surveys, which while forming a very heterogeneous sample suggest the following, at least statistically.

(i) There appears to be no large difference in the spin temperature/covering factor ratio between the low- and high-redshift DLAs

(Fig. 11 and Table 3), although the non-detections do have a higher mean redshift and more sensitive observations of these would be required to fully address this. Nevertheless, the fact that the mean T_{spin}/f difference is largest for a redshift partition of $z_{\text{CUT}} = 1.0$ is consistent with the geometry effects noted by Curran & Webb (2006). Other factors, such as increasing WNM fractions (increasing T_{spin}) or an evolution in morphologies (also decreasing f) with redshift cannot be ruled out, although the T_{spin}/f degeneracy cannot be broken.

(ii) The observations since Curran et al. (2005) confirm that the 21-cm line strength is correlated with the total neutral hydrogen column density, which further suggests that the spin temperature to covering factor ratio (T_{spin}/f) is *roughly* constant, for both the detections and non-detections (Fig. 12).

(iii) By combining the radio source sizes with the angular diameter distances to the DLAs, we show that the absorber extent normalized by the covering factor (d_{abs}/\sqrt{f}) is correlated with the line-strength for the detections, with the non-detections generally exhibiting larger values of d_{abs}/\sqrt{f} (Fig. 15). A possible interpretation is that the non-detections require larger minimum absorber extents in order to be detected. This may also be interpreted as the covering factors being lower than for the detections.

This argument relies on the assumption that the unknown morphologies of the non-detections are not those of spiral galaxies. This is consistent with *both* the hypotheses of Kanekar & Chengalur (2003) and Curran et al. (2005), in that spiral galaxies may have lower spin temperatures or larger covering factors than the other morphologies, respectively. The constancy of T_{spin}/f between the detections and non-detections (point ii, above) may suggest that both contribute, with lower covering factors being balanced by lower spin temperatures. The absorber extent–line strength correlation further suggests that $d_{\text{abs}} \propto f^{3/2}/T_{\text{spin}}$ for the detections. Although, once again, we are limited by the spin temperature/covering factor degeneracy, we do believe that the large scatter in this ($T_{\text{spin}}/f = 60$ to $\gtrsim 13\,000$ K) is mainly dominated, or at least balanced, by different covering factors: this represents a vast range of spin temperatures (specifically, $T_{\text{spin}} \approx 200$ to $\gtrsim 9\,000$ K suggested by Kanekar & Chengalur 2003). Although having a much smaller dynamic range than the spin temperature, the covering factor is subject to three separate effects – the extent of the absorbing region, the size and morphology of the background 1.4-GHz emitter, and the effects introduced by the geometry of a flat expanding Universe. Furthermore, the beam filling of the cold neutral medium in these absorbers could have a significant effect on both the covering factor and the spin temperature.

(iv) We agree with the suspicions of York et al. (2007) that the $z_{\text{abs}} = 2.289$ absorber towards 0311+430 arises within a spiral galaxy. Although not on the basis of its low spin temperature (which we do not find unusual at these redshifts), but on its absorption cross-section and its grouping with the other spirals on a line-strength–metallicity plot.

ACKNOWLEDGMENTS

We would like to thank the anonymous referees for their prompt and helpful comments, Ishwara Chandra for his assistance with the GMRT observations and Jayaram Chengalur for his perseverance in getting the data to us in a format which MIRIAD could handle. Thanks also to Nadia Lo for her IDL expertise, which assisted greatly with the GBT data reduction and to Warren Trotman (wherever he may

be) for the figure of the little telescope (in Fig. 14), which SJC has used since our Masters write-up days at Jodrell Bank.

This research has made use of the NASA/IPAC Extragalactic Data base (NED) which is operated by the Jet Propulsion Laboratory, California Institute of Technology, under contract with the National Aeronautics and Space Administration. This research has also made use of NASA’s Astrophysics Data System Bibliographic Service and ASURV Rev 1.2 (Lavalley, Isobe & Feigelson 1992), which implements the methods presented in Isobe, Feigelson & Nelson (1986).

MTM thanks the Australian Research Council for a QEII Research Fellowship (DP0877998).

REFERENCES

Bahcall J. N., Ekers R. D., 1969, *ApJ*, 157, 1055
 Bajtlik S., Duncan R. C., Ostriker J. P., 1988, *ApJ*, 327, 570
 Baker A. C., Mathlin G. P., Churches D. K., Edmunds M. G., 2000, in Favata F., Kaas A., Wilson A., eds, *ESA SP, Vol. 45, Star Formation from the Small to the Large Scale, the Chemical Evolution of the Universe*. ESA, Noordwijk, p. 21
 Beasley A. J., Gordon D., Peck A. B., Petrov L., MacMillan D. S., Fomalont E. B., Ma C., 2002, *ApJS*, 141, 13
 Briggs F. H., Wolfe A. M., 1983, *ApJ*, 268, 76
 Briggs F. H., Brinks E., Wolfe A. M., 1997, *AJ*, 113, 467
 Carilli C. L., Lane W., de Bruyn A. G., Braun R., Miley G. K., 1996, *AJ*, 111, 1830
 Chen H.-W., Lanzetta K. M., 2003, *ApJ*, 597, 706
 Curran S. J., 2009, *MNRAS*, submitted (arXiv:0910.3998)
 Curran S. J., Webb J. K., 2006, *MNRAS*, 371, 356
 Curran S. J., Murphy M. T., Pihlström Y. M., Webb J. K., Purcell C. R., 2005, *MNRAS*, 356, 1509
 Curran S. J., Tzanavaris P., Murphy M. T., Webb J. K., Pihlström Y. M., 2007a, *MNRAS*, 381, L6
 Curran S. J., Tzanavaris P., Pihlström Y. M., Webb J. K., 2007b, *MNRAS*, 382, 1331
 Curran S. J., Webb J. K., Murphy M. T., Bandiera R., Corbelli E., Flambaum V. V., 2002, *PASA*, 19, 455
 Curran S. J., Webb J. K., Murphy M. T., Carswell R. F., 2004, *MNRAS*, 351, L24
 Curran S. J., Whiting M. T., Wiklind T., Webb J. K., Murphy M. T., Purcell C. R., 2008, *MNRAS*, 391, 765
 Dalgarno A., McCray R. A., 1972, *Annu. Rev. Astron. Astrophys.*, 10, 375
 de Bruyn A. G., O’Dea C. P., Baum S. A., 1996, *A&A*, 305, 450
 Dickey J. M., Lockman F. J., 1990, *ARA&A*, 28, 215
 Douglas J. N., Bash F. N., Bozyan F. A., Torrence G. W., Wolfe C., 1996, *AJ*, 111, 1945
 Ellison S. L., Yan L., Hook I. M., Pettini M., Wall J. V., Shaver P., 2001, *A&A*, 379, 393
 Field G. B., 1959, *ApJ*, 129, 536
 Fomalont E. B., Frey S., Paragi Z., Gurvits L. I., Scott W. K., Taylor A. R., Edwards P. G., Hirabayashi H., 2000, *ApJS*, 131, 95

Gupta N., Srianand R., Petitjean P., Noterdaeme P., Saikia D. J., 2009, *MNRAS*, 398, 201
 Gurvits L. I., Kellermann K. I., Frey S., 1999, *A&A*, 342, 378
 Harvanek M., Stocke J. T., Morse J. A., Rhee G., 1997, *AJ*, 114, 2240
 Isobe T., Feigelson E., Nelson P., 1986, *ApJ*, 306, 490
 Jorgenson R. A., Wolfe A. M., Prochaska J. X., Carswell R. F., 2009, *ApJ*, 704, 247
 Kanekar N., Chengalur J. N., 2001, *MNRAS*, 325, 631
 Kanekar N., Chengalur J. N., 2003, *A&A*, 399, 857
 Kanekar N., Chengalur J. N., Lane W. M., 2007, *MNRAS*, 375, 1528
 Kanekar N., Lane W. M., Momjian E., Briggs F. H., Chengalur J. N., 2009a, *MNRAS*, 394, L61
 Kanekar N., Prochaska J. X., Ellison S. L., Chengalur J. N., 2009b, *MNRAS*, 396, 385
 Kanekar N., Subrahmanyam R., Ellison S. L., Lane W., Chengalur J. N., 2006, *MNRAS*, 370, L46
 Lanfranchi G. A., Friaça A. C. S., 2003, *MNRAS*, 343, 481
 Lavalley M. P., Isobe T., Feigelson E. D., 1992, *BAAS*, 24, 839
 Le Brun V., Bergeron J., Boissé P., Deharveng J. M., 1997, *A&A*, 321, 733
 Lu L., Sargent W. L. W., Barlow T. A., Churchill C. W., Vogt S. S., 1996, *ApJS*, 107, 475
 Möller P., Fynbo J. P. U., Fall S. M., 2004, *A&A*, 422, L33
 Murphy M. T., Curran S. J., Webb J. K., 2004, in Duc P.-A., Braine J., Brinks E., eds, *Proc. IAU Symp. 217, Recycling Intergalactic and Interstellar Matter*. Astron. Soc. Pac., San Francisco, p. 252
 Murphy M. T., Curran S. J., Webb J. K., Ménager H., Zych B. J., 2007, *MNRAS*, 376, 673
 Noterdaeme P., Ledoux C., Petitjean P., Srianand R., 2008, *A&A*, 481, 327
 Prochaska J. X., Herbert-Fort S., 2004, *PASP*, 116, 622
 Prochaska J. X., Gawiser E., Wolfe A. M., Castro S., Djorgovski S. G., 2003, *ApJ*, 595, L9
 Prochaska J. X., Herbert-Fort S., Wolfe A. M., 2005, *ApJ*, 635, 123
 Rao S., Nestor D. B., Turnshek D., Lane W. M., Monier E. M., Bergeron J., 2003, *ApJ*, 595, 94
 Rao S., Turnshek D., Nestor D. B., 2006, *ApJ*, 636, 610
 Rao S. M., Prochaska J. X., Howk J. C., Wolfe A. M., 2005, *AJ*, 129, 9
 Srianand R., Petitjean P., Ledoux C., Ferland G., Shaw G., 2005, *MNRAS*, 362, 549
 Stanghellini C., Baum S. A., O’Dea C. P., Morris G. B., 1990, *A&A*, 233, 379
 Steidel C. C., Bowen D. V., Blades J. C., Dickenson M., 1995, *ApJ*, 440, L45
 Tingay S. J. et al., 1998, *ApJ*, 497, 594
 Turnshek D. A., Bohlin R. C., 1993, *ApJ*, 407, 60
 Turnshek D. A., Wolfe A. M., Lanzetta K. M., Briggs F. H., Cohen R. D., Foltz C. B., Smith H. E., Wilkes B. J., 1989, *ApJ*, 344, 567
 Wolfe A. M., Burbidge G. R., 1975, *ApJ*, 200, 548
 Wolfe A. M., Gawiser E., Prochaska J. X., 2005, *ARA&A*, 43, 861
 Wolfire M. G., Hollenbach D., McKee C. F., Tielens A. G. G. M., Bakes E. L. O., 1995, *ApJ*, 443, 152
 York B. A., Kanekar N., Ellison S. L., Pettini M., 2007, *MNRAS*, 382, L53

This paper has been typeset from a $\text{\TeX}/\text{\LaTeX}$ file prepared by the author.